



ISTITUTO NAZIONALE DI RICERCA METROLOGICA Repository Istituzionale

Effective versus standard Epstein loss figure in Fe-Si sheets.

This is the author's accepted version of the contribution published as:

Original

Effective versus standard Epstein loss figure in Fe-Si sheets / Ferrara, Enzo; Appino, Carlo; Rocchino, Luciano; Ragusa, Carlo; de la Barrière, Olivier; Fiorillo, Fausto. - In: INTERNATIONAL JOURNAL OF APPLIED ELECTROMAGNETICS AND MECHANICS. - ISSN 1383-5416. - 55:(2017). [10.3233/JAE-172263]

Availability:

This version is available at: 11696/57002 since: 2021-02-07T06:36:20Z

Publisher:

IOS Press:Nieuwe Hemweg

Published

DOI:10.3233/JAE-172263

Terms of use:

This article is made available under terms and conditions as specified in the corresponding bibliographic description in the repository

Publisher copyright

(Article begins on next page)

Effective versus standard Epstein loss figure in Fe-Si sheets.

Enzo Ferrara¹, Carlo Appino¹, Luciano Rocchino¹, Carlo Ragusa²,
Olivier de la Barrière³, and Fausto Fiorillo¹

¹ *Istituto Nazionale di Ricerca Metrologica, Nanoscience and Materials Division, Torino, Italy*

² *Politecnico di Torino, Energy Department, Torino, Italy*

³ *SATIE-ENS, UniverSud, Cachan, France*

Abstract

The magnetic power losses have been measured at 50 Hz and different peak polarization values on different types of non-oriented and grain-oriented Fe-Si sheets using the Epstein frame, according to the current standards. The very same measurements have then been repeated by measuring polarization and tangential magnetic field by means of localized windings, centrally placed on the strips inside the Epstein frame windings, thereby retrieving the effective field and the true power loss figure. It is obtained that the ratio of the standard P_{epst} to the effective P_{eff} loss figure, which can be interpreted in terms of ratio of effective l_{eff} to conventional ($l_m = 0.94$ m) magnetic path length, evolves with the peak polarization J_p , showing, in general, a monotonic increase with increasing J_p . The deviation of P_{epst} from P_{eff} is observed to range from about -3 % in the non-oriented alloys at low inductions to about +5 % in the grain-oriented alloys at $J_p = 1.8$ T. This behavior finds a rationale in the existence of a polarization profile $J_p(x)$ measured along the strip length and in the dependence of P_{eff} on J_p , showing a power law $P_{\text{eff}}(J_p) \propto J_p^n$, with $n > 1$ and increasing with J_p . The so calculated effective path length $l_{\text{eff}} = l_m \cdot P_{\text{epst}} / P_{\text{eff}}$ consistently show a monotonic increase with J_p , which is more relevant in the GO alloys.

Keywords: Magnetic power losses, Epstein frame, Magnetic steels.

32 1. Introduction

33 The 25 cm Epstein test-frame with a defined magnetic path length $l_m = 0.94$ m is a solidly assessed method for
34 the characterization of the magnetic steel sheets. It ensures good measurement reproducibility and is widely
35 adopted as an industry standard [1][2][3][4]. It is also well established that the specific features of the employed
36 magnetic circuit, with the double overlapping corners and the ensuing inhomogeneous flux distribution, make the
37 value of the measured quantities, namely the magnetic losses, different from the value of the true quantities [5][6].
38 True values could, however, be possibly accounted for by incorporating the complex response of the magnetic
39 circuit into an effective magnetic path length l_{eff} , depending on the type of sheet, peak induction value, frequency,
40 and type of excitation [7]. Should the effective (true) power loss figure P_{eff} be measured, one could express it in
41 terms of standard power loss value P_{epst} according to

$$42 \quad P_{\text{eff}} = P_{\text{epst}} \cdot l_m / l_{\text{eff}}. \quad (1)$$

43 Measurements of P_{eff} using a single strip tester and an H -coil were reported for non-oriented (NO) and
44 grain-oriented (GO) sheets by Ahlers, et al. [8]. They found at 50 Hz $P_{\text{epst}} < P_{\text{eff}}$, that is $l_{\text{eff}} > l_m$ in all materials,
45 with maximum difference of the order of 8% in GO sheets at $J_p = 1.7$ T. These authors justified their results in
46 terms of effective length, expressed as $l_{\text{eff}} = l_0 + (\mu_l/2\mu_c) \cdot l_c$, the sum of the legs length l_0 and part of the corners
47 length l_c , depending on the ratio of the leg to corner permeabilities μ_l and μ_c . A number of literature experiments
48 [5] actually show scattered outcomes, both in NO and GO materials, with P_{epst} either higher or lower than P_{eff} and
49 $P_{\text{epst}} / P_{\text{eff}}$ generally decreasing with the peak polarization J_p . Marketos, et al. [7][9] have determined l_{eff} by
50 measuring GO and NO sheets with conventional 25 cm and reduced 17.5 cm Epstein frames. They find, assuming
51 identical flux distribution in the corners of the two frames, that l_{eff} is always higher than l_m (that is, $P_{\text{epst}} / P_{\text{eff}} > 1$)
52 in GO high-permeability sheets and, in contrast with the results reported in [5], increasing with J_p .

53 In this paper we discuss measurements of power losses performed at 50 Hz on different types of NO and GO
54 steel sheets, both according to the measuring standard (25 cm Epstein frame with $l_m = 0.94$ m) and by detecting
55 the tangential field and the induction derivative by collinear narrow H - and B -coils windings, placed directly upon
56 the steel strips at the centre of the Epstein legs. In this way, the true power loss $P_{\text{eff}}(J_p)$ is obtained in comparison
57 with the standard loss figure $P_{\text{epst}}(J_p)$. A ratio $P_{\text{epst}} / P_{\text{eff}}$ monotonically increasing with J_p is thus found in all
58 materials. This can equivalently be expressed in terms of an effective path length similarly increasing with J_p .

59 2. Experimental method

61 The magnetic measurements were performed at 50 Hz under sinusoidal induction waveform on the NO and GO
62 alloys listed in Table 1. Both conventional (CGO) and high-permeability (HGO) grain-oriented sheets were
63 investigated. A calibrated hysteresisgraph-wattmeter with digital control of the induction waveform was used,
64 where signal acquisition and A/D conversion is made by means of a 12-bit 500 MHz HDO4054 LeCroy
65 oscilloscope. The whole measuring process is performed within an Agilent VEE environment. The NO and GO
66 alloys were tested in the polarization intervals 0.5 T – 1.5 T and 1.0 T – 1.8 T, respectively, with either eight or

67 twelve strips inserted in the Epstein frame, depending on the sheet thickness. For any given material, a standard
 68 measurement was first made, followed by measurements with the centrally placed local windings. The
 69 arrangement of the 17 mm wide H - and B -coils, which are stuck together and placed inside the Epstein windings,
 70 is schematically shown in Fig. 1. The H -coil (turn-area $N_{\text{H}}S_{\text{H}} = 2.11 \cdot 10^{-2} \text{ m}^2$, thickness $\sim 1.5 \text{ mm}$) is made of a few
 71 hundred turns (wire diameter 0.05 mm) wound on a rigid fibreglass plate and calibrated inside a field reference
 72 setup [10]. The 50-turn B -coil enwraps the H -coil and the strips under test. The air-flux contribution is usually
 73 negligible, but it is in any case compensated via software. Once the single standard Epstein measurement of the
 74 power loss $P_{\text{epst}}(J_{0\text{p}})$ at a given polarization $J_{0\text{p}}$ is done, the local $\text{d}B/\text{d}t$ and $\text{d}H_{\text{eff}}/\text{d}t$ signals are simultaneously
 75 detected, under the identical exciting conditions, at a significant number of points, from corner to corner, along
 76 the length of the Epstein leg, amplified by calibrated low-noise amplifiers SR560, and integrated. These local
 77 measurements are then identically repeated on the other legs and the results are averaged. They provide the
 78 behaviours of $J(x)$ and $H_{\text{eff}}(x)$ as a function of the distance x from the centre of the leg for the Epstein measured
 79 polarization $J_{0\text{p}}$. The distance x ranges between -110 mm and +110 mm. Finally, the H - and B -coils are moved to
 80 the centre of the leg ($x = 0$) and the measurement of $P_{\text{eff}}(J_{0\text{p}})$ is performed by imposing the local $\text{d}J/\text{d}t$ sinusoidal
 81 with peak polarization value $J_{\text{p}}(0) = J_{0\text{p}}$. It is remarked that across the 17 mm wide region occupied by the coils
 82 centred at $x = 0$ the polarization is highly uniform. Given the low field levels involved, a certain background noise
 83 in the $\text{d}H_{\text{eff}}/\text{d}t$ signal is inevitable. This is dealt with by repeating the very same measurement a number of times,
 84 to make the random uncertainty contribution negligible. The process is further repeated on the other legs and the
 85 results are averaged.

86

87

88 3. Experimental results and discussion

89 The general outcome of the measurements performed on the six different types of soft magnetic steels
 90 described in Table 1, two NO sheets of thickness 0.194 mm and 0.343 mm, two conventional and two high-
 91 permeability GO sheets, of thickness ranging between 0.255 and 0.295 mm, is that the standard Epstein loss figure
 92 P_{epst} can either overestimate or underestimate the effective power loss P_{eff} , but the ratio $P_{\text{epst}} / P_{\text{eff}}$ is always a
 93 monotonically increasing function of J_{p} . **The local $J_{\text{p}} = J_{\text{p}}(0)$ value involved in the measurement of P_{eff} is obviously**
 94 **made to coincide with the polarization value $J_{0\text{p}}$ previously determined through the whole Epstein secondary**
 95 **winding.** While this result may appear partly ad odd with previous literature outcomes [5][8], we shall observe in
 96 the following how the behavior of $P_{\text{epst}} / P_{\text{eff}}$ can be justified in terms of inhomogeneity of the induction along the
 97 Epstein legs **and the power law dependence** of P_{eff} on J_{p} . Let us therefore observe in Fig. 2 the overall experimental
 98 behaviors of $(P_{\text{epst}} - P_{\text{eff}}) / P_{\text{eff}}$ versus J_{p} and of the related effective magnetic path length $l_{\text{eff}} = l_{\text{m}} \cdot (P_{\text{epst}} / P_{\text{eff}})$. **Similar**
 99 **trends versus J_{p} are followed by the NO and GO materials, but the standard power loss P_{epst} becomes significantly**
 100 **higher, around 4 % – 5 %, than the true loss P_{eff} at the highest J_{p} values in the GO sheets.** Table 2 provides a
 101 comparison of the measured power losses P_{epst} and P_{eff} .

102 In order to find a rationale for the J_{p} dependent relationship between P_{epst} and P_{eff} , it is useful to analyze the

103 distribution of field and polarization along the magnetic circuit, as retrieved by the previously described local
 104 measurements. To start with, we provide an example in Fig. 3, concerning the NO-2 sheet, of field decomposition
 105 along a leg of the frame for a standard Epstein measurement at a given polarization value J_p . The solenoid
 106 surrounding each leg has length $2L = 195$ mm. By subtracting the effective field $H_{\text{eff}}(x)$, measured by sliding the
 107 H -coil along the leg, from the field $H_{\text{sol}}(x)$ applied by the primary solenoid, we obtain the behavior of the
 108 magnetostatic field $H_d(x)$. This exerts a demagnetizing action towards the strip portion of length $2L$ underlying the
 109 Epstein winding, adding instead to H_{sol} towards the corners, to eventually impose a magnetic path length l_{eff} longer
 110 than the solenoid length. The effect of H_d is less important at high inductions, where the permeability is lower and
 111 the free poles are more localized around the solenoid edges. The distribution of the polarization $J_p(x)$ along $2L$ is
 112 however moderately affected, as shown by the examples regarding the samples NO-2 and HGO-1 shown in Fig.
 113 4. These curves are representative of the flux distribution found in all materials and bring to light the fact that,
 114 because of the strong non-linear dependence of the power loss on J_p , the true loss value cannot be recovered by a
 115 standard Epstein measurement, adjusted through a simple constant (in this case the conventional magnetic path
 116 length l_m). By denoting the polarization measured through the secondary Epstein winding $J_0(t) = J_{0p} \sin(\omega t)$,

117 where $J_{0p} = \frac{1}{2L} \int_{-L}^L J_p(x) dx$, we can write the power loss per unit volume measured with the standard method

$$118 \quad P_{\text{epst}}(J_{0p}) = \frac{1}{T} \int_0^T H_{\text{epst}}(t) \cdot J_{0p} \omega \cos(\omega t) dt, \quad (2)$$

119 where $H_{\text{epst}}(t) = N_H i_H(t) / l_m$, N_H is the number of turns of the primary winding and $i_H(t)$ is the magnetizing current.
 120 The true power loss corresponding to the condition met with the standard Epstein measurement is therefore given
 121 by the average of the local $P_{\text{eff}}(x)$ across the length $2L$

$$122 \quad P_{\text{eff}}(J_{0p}) = \frac{1}{2L} \int_{-L}^L dx \frac{1}{T} \int_0^T H_{\text{eff}}(t, x) \cdot J_p(x) \cdot \omega \cos(\omega t) dt = \frac{1}{2L} \int_{-L}^L P_{\text{eff}}(J_p(x)) dx. \quad (3)$$

123 We thus obtain the effective magnetic path length corresponding to such condition

$$124 \quad l_{\text{eff}}(J_{0p}) = l_m \cdot \frac{P_{\text{epst}}(J_{0p})}{P_{\text{eff}}(J_{0p})}. \quad (4)$$

125 The quantity $P_{\text{eff}}(J_{0p})$ can be measured, according to Eq. (3), by integrating the previously discussed local
 126 measurements, which are represented as a function of J_p in Fig. 5, over the $J_p(x)$ distribution shown in Fig. 4. This
 127 is easily done through knowledge of the measured dependence of $P_{\text{eff}}(J_p)$ on J_p , which, as shown in Fig. 5, follows
 128 a power law $P_{\text{eff}}(J_p) \propto J_p^n$, with n an increasing function of J_p . By introducing the $P_{\text{eff}}(J_{0p})$ calculated by Eq. (3), we
 129 obtain the behavior of $l_{\text{eff}}(J_{0p})$ in the different materials shown in Fig. 6. On the other hand, the previously defined
 130 $P_{\text{eff}}(J_p)$ (Fig. 2) is the true loss measured at $x = 0$ when $J_p(0) = J_p$, which is compared with the Epstein power loss
 131 when the secondary winding provides the same polarization value J_p . $l_{\text{eff}}(J_p)$ is correspondingly defined through
 132 Eq. (1). Consequently, $l_{\text{eff}}(J_{0p})$ and $l_{\text{eff}}(J_p)$ do not usually coincide. $l_{\text{eff}}(J_{0p})$ is, in any case, the magnetic path length
 133 to be applied in substitution of l_m when making the standard Epstein testing at 50 Hz at the specific measured

134 polarization level J_{0p} . It takes into account the fact that the peak polarization J_{0p} measured by the secondary Epstein
135 winding is the average of $J_p(x)$ between $\pm L$, according to the behaviors of $J_p(x)$ shown in Fig. 4. It will coincide
136 with $l_{\text{eff}}(J_p)$ for homogeneous $J_p(x)$ across the solenoid length $2L$, a limiting unattainable condition. The calculated
137 $l_{\text{eff}}(J_{0p})$ and the measured $l_{\text{eff}}(J_p)$ nevertheless display quite similar increasing trends vs. J_p , both in NO and GO
138 alloys, as illustrated by their behaviors shown in Fig. 6. **It is appreciated the fact that, as shown in Figs. 2 and 6,**
139 **the effective magnetic path length in the GO alloys tends to be higher than in the NO sheets, besides being larger**
140 **than the conventional Epstein value $l_m = 0.94$ m. This implies that $P_{\text{epst}} / P_{\text{eff}}$ is similarly higher. The present results**
141 **actually show that $J_p(x)$ is more homogeneous in the GO strips (see the example shown in Fig. 4), thereby better**
142 **approaching the ideal condition of perfectly homogeneous magnetization over the whole 1m long Epstein circuit.**
143

144 4. Conclusions

145 Measurements of the true power losses in different types of non-oriented and grain-oriented materials
146 using localized H - and B -coils placed inside the legs of a standard 25 cm Epstein frame have been compared,
147 upon a range of peak polarization values, with the loss figures obtained according to the usual procedure
148 prescribed by the measuring standards. It is found that true P_{eff} and standard P_{epst} power loss figures are in a
149 relationship dependent on the imposed peak polarization value J_p , with the ratio $P_{\text{epst}} / P_{\text{eff}}$ exhibiting a
150 monotonical increase with J_p in all materials in the investigated polarization range $0.5 \text{ T} \leq J_p \leq 1.8 \text{ T}$. This
151 behavior, which can be interpreted in terms of an effective magnetic path length l_{eff} , to be used as a substitute for
152 the conventional fixed length $l_m = 0.94$ m in the expression for the applied field, is justified in terms of non-
153 uniform profile of the polarization $J_p(x)$ along the strip portion underlying the Epstein secondary winding and
154 non-linear increase of P_{eff} with J_p . The effective path length $l_{\text{eff}}(J_p)$ can then be calculated, by which true and
155 Epstein power losses are reconciled.

156

157

158

159

160

161

162

163

164

165

166

167

168

169

170
171
172
173
174
175
176
177
178
179
180
181
182
183
184
185
186
187
188
189
190
191
192
193
194
195
196
197
198
199
200
201
202
203
204
205
206
207
208
209
210
211

References

- [1] J. Sievert, H. Ahlers, F. Fiorillo, L. Rocchino, M. Hall and L. Henderson, Magnetic measurements on electrical steels using Epstein and SST method, *PTB-Bericht E-74*(2001), 1–28.
- [2] C. Appino, E. Ferrara, F. Fiorillo, L. Rocchino, C. Ragusa, J. Sievert, T. Belgrand, C. Wang, P. Denke, S. Siebert, Y. Norgren, K. Gramm, S. Norman, R. Lyke, M. Albrecht, X. Zhou, W. Fan, X. Guo, M. Hall, “International comparison on SST and Epstein measurements in grain-oriented Fe-Si sheet steel”, *Int. J. Appl. Electromagnetics Mech.* **48** (2015), 123-133, doi: 10.3233/JAE-151978.
- [3] IEC Standard Publication 60404-2, Methods of measurement of the magnetic properties of electrical steel sheet and strip by means of the Epstein frame, (Geneva: IEC Central Office, 1996).
- [4] ASTM Publication A343.97, Standard test method for alternating-current magnetic properties of amorphous materials at power frequencies using wattmeter-ammeter-voltmeter method using wattmeter-ammeter-voltmeter method and 25-cm Epstein test frame” (West Conshohocken, PA: ASTM International, 1993).
- [5] J.D. Sievert, Determination of the AC magnetic power loss of electrical steel sheet: present status and trends, *IEEE Trans. Magn.* **20** (1984), 1702-1706, doi: [10.1109/TMAG.1984.1063278](https://doi.org/10.1109/TMAG.1984.1063278).
- [6] E. Antonelli, E. Cardelli, A. Faba, Epstein frame: how and when it can be really representative about the magnetic behavior of laminated magnetic steels, *IEEE Trans. Magn.* **41** (2005), 1516-1519, doi: [10.1109/TMAG.2005.845072](https://doi.org/10.1109/TMAG.2005.845072).
- [7] P. Marketos, S. Zurek, and A.J. Moses, A method for defining the mean path length of the Epstein frame, *IEEE Trans. Magn.* **43** (2007), 2755-2757, doi: [10.1109/TMAG.2007.894124](https://doi.org/10.1109/TMAG.2007.894124).
- [8] H. Ahlers, J.D. Sievert, and Qu.-ch. Qu, Comparison of a single strip tester and Epstein frame measurements, *J. Magn. Magn. Mater.* **26** (1982), 176-178, doi:10.1016/0304-8853(82)90145-7.
- [9] P. Marketos, S. Zurek, and A.J. Moses, Calculation of the mean path length of the Epstein frame under non-sinusoidal excitations using the double Epstein method, *J. Magn. Magn. Mater.*, **320** (2008), 2542-2545, doi: [10.1016/j.jmmm.2008.04.085](https://doi.org/10.1016/j.jmmm.2008.04.085).
- [10] F. Fiorillo, G.F. Durin, and L. Rocchino: “A reference system for the measurement of low-strength magnetic flux density”, *J. Magn. Magn. Mater.*, **304** (2006), e540-e542.

212
213
214
215
216
217
218
219
220
221
222
223
224
225
226
227
228
229
230
231
232
233
234
235
236
237
238
239
240
241
242
243
244
245
246
247
248
249
250
251
252
253
254
255
256
257
258
259
260
261
262
263
264

Table 1

Physical parameters of the investigated non-oriented (NO), conventional (CGO) and high-permeability (HGO) grain-oriented steel sheets.

Fe-Si alloy	Composition	Thickness (mm)	Density (kg/m ³)	Resistivity (mΩm)
NO-1	Fe-(3.2 wt%)Si	0.194	7650	52·10 ⁻⁸
NO-2	Fe-(3.5 wt%)Si	0.343	7600	56.4·10 ⁻⁸
CGO-1	Fe-(3 wt%)Si	0.255	7650	48·10 ⁻⁸
CGO-2		0.261		
HGO-1		0.257		
HGO-2		0.295		

265
266
267
268
269
270
271
272
273
274
275
276
277
278
279
280
281
282
283
284
285
286
287

Table 2

Power loss at 50 Hz obtained by the standard Epstein measurement (P_{epst}) and the localized measurement (P_{eff}) as a function of peak polarization on three different Fe-Si sheets.

$f = 50$ Hz	NO-1		CGO-2		HGO-1	
J_p (T)	P_{epst} (W/kg)	P_{eff} (W/kg)	P_{epst} (W/kg)	P_{eff} (W/kg)	P_{epst} (W/kg)	P_{eff} (W/kg)
0.50	0.241	0.248	--	--	--	--
0.75	0.480	0.489	--	--	--	--
1.0	0.784	0.755	0.345	0.343	0.303	0.299
1.2	1.125	1.135	0.499	0.498	0.431	0.426
1.4	1.656	1.665	--	--	--	--
1.5	2.07	2.050	0.811	0.787	0.681	0.664
1.7	--	--	1.198	1.154	0.914	0.874
1.8	--	--	1.587	1.514	1.123	1.063

288
289
290
291
292
293
294
295
296
297
298
299
300
301
302
303
304
305
306

Figure captions

307
308
309
310
311
312
313
314
315
316
317
318
319
320
321
322
323
324
325
326
327
328
329
330
331
332
333
334
335
336
337
338
339
340
341
342
343
344
345
346
347
348
349
350
351
352
353
354
355
356
357

Fig. 1 – Arrangement of the local sensing coils inside a leg of the Epstein frame. The flat multiturn H -coil (thickness ~ 1.5 mm) is placed in contact with the Epstein strip surface and the B -coil is wound around it and the steel strips. The coils are about 17 mm wide and can slide along the whole length of the Epstein leg.

Fig. 2 – The experimental dependence on J_p of the ratio of standard to true power losses $P_{\text{epst}}/P_{\text{eff}}$ in NO and in conventional (CGO) and high-permeability (HGO) Fe-Si alloys (a) is paralleled by the behavior of the effective magnetic path length l_{eff} (b).

Fig. 3 – Effective field H_{eff} measured versus the distance x from the Epstein leg centre in the NO-2 sheet. It is $H_{\text{eff}} = H_{\text{sol}} - H_d$, the difference between the field H_{sol} generated by the primary winding and the field H_d originating from the free poles distributed along the strip length. To note the demagnetizing and magnetizing effect of H_d beneath and outside the solenoid length. The horizontal dotted line shows the conventional field H_{epst} , calculated assuming the magnetic path length $l_m = 0.94$ m.

Fig. 4 – Examples of measured distribution of the reduced polarization $J(x) / J(0)$ upon the portion of strip length underlying the Epstein secondary winding in the NO-2 and HGO-1 sheets.

Fig. 5 – The measured effective power loss $P_{\text{eff}}(J_p)$ increases with the peak polarization J_p according to a power law $P_{\text{eff}} \propto J_p^n$, with n an increasing function of J_p .

Fig. 6 – Effective magnetic path lengths $l_{\text{eff}}(J_{0p})$ and $l_{\text{eff}}(J_p)$ versus peak polarization in the investigated NO and GO steel sheets. $l_{\text{eff}}(J_{0p})$ is calculated through Eqs. (2)–(4). It permits one to retrieve the true power loss value from the standard loss figure for peak polarization J_{0p} measured with the secondary Epstein winding. $l_{\text{eff}}(J_p)$ is the same quantity obtained for $J_p = J_p(0)$, where $J_p(0)$ is the polarization measured at the centre of the Epstein leg.

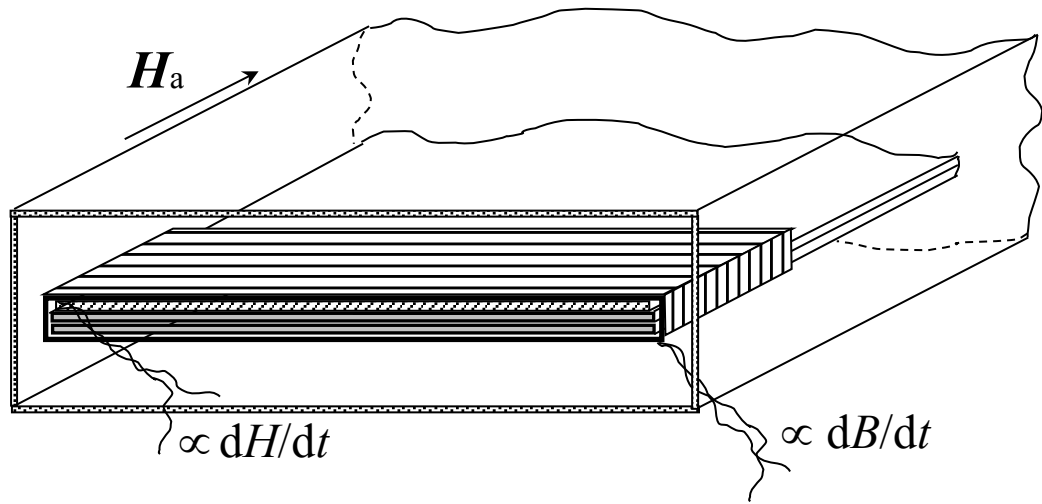
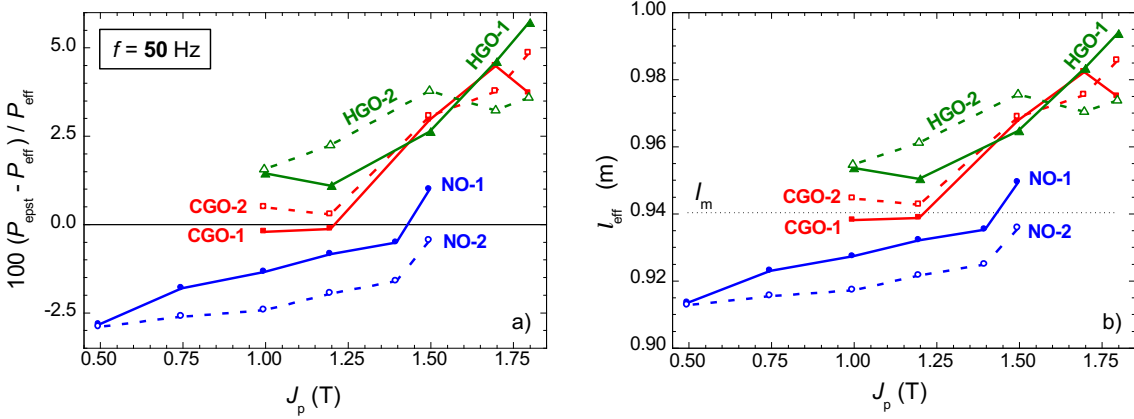


Fig. 1 – Arrangement of the local sensing coils inside a leg of the Epstein frame. The flat multiturn H -coil (thickness ~ 1.5 mm) is placed in contact with the Epstein strip surface and the B -coil is wound around it and the steel strips. The coils are about 17 mm wide and can slide along the whole length of the Epstein leg.

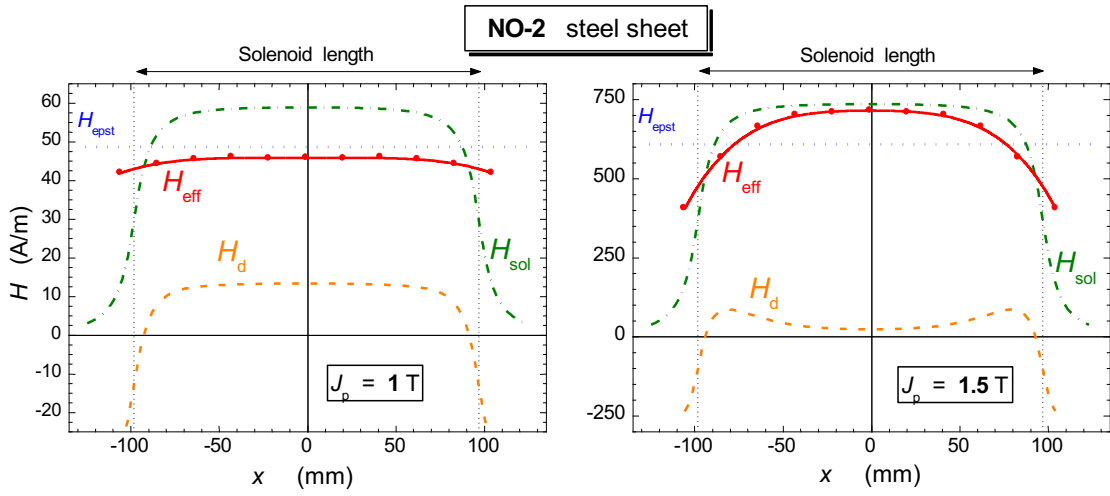
408
 409
 410
 411
 412
 413
 414
 415
 416



417
 418
 419
 420
 421
 422
 423
 424
 425
 426
 427
 428
 429
 430
 431
 432
 433
 434
 435
 436
 437
 438
 439

Fig. 2 – The experimental dependence on J_p of the ratio of standard to true power losses P_{epst}/P_{eff} in NO and in conventional (CGO) and high-permeability (HGO) Fe-Si alloys (a) is paralleled by the behavior of the effective magnetic path length l_{eff} (b).

440
441
442
443
444
445
446



447
448
449
450
451
452
453
454
455
456
457
458
459
460
461
462
463
464
465

leg 466
 H_{sol} 467
les 468
ing 469
ine 470
gth 471
472
473
474
475
476
477
478
479
480
481
482
483
484
485
486
487
488

489
490
491
492
493
494
495
496
497
498
499
500
501
502
503
504
505
506
507
508
509
510
511
512
513
514
515
516
517
518
519
520
521
522
523
524
525
526
527
528
529
530
531
532
533
534
535
536
537

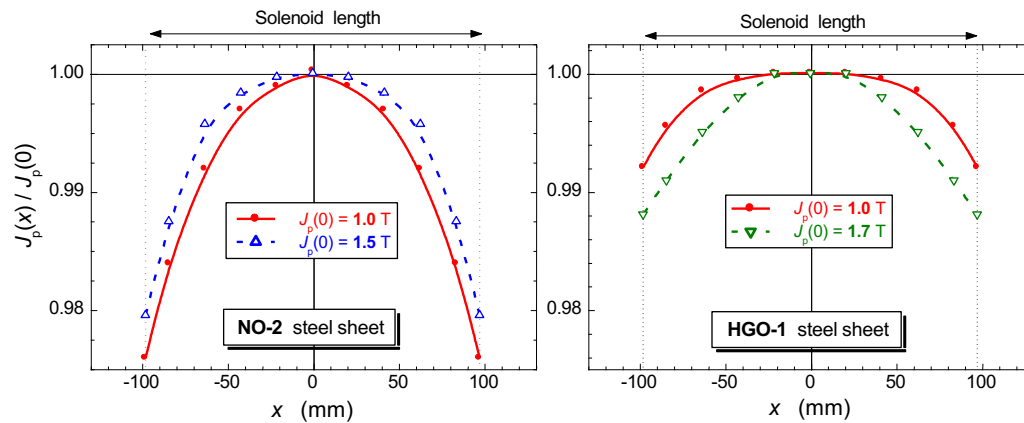


Fig. 4 – Examples of measured distribution of the reduced polarization $J(x) / J(0)$ upon the portion of strip length underlying the Epstein secondary winding in the NO-2 and HGO-1 sheets.

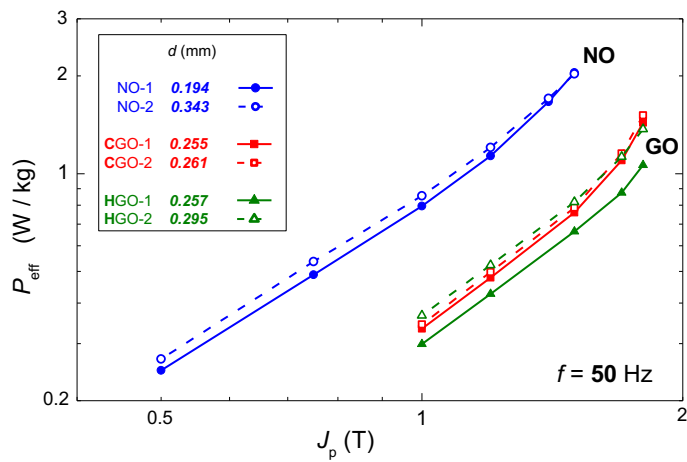
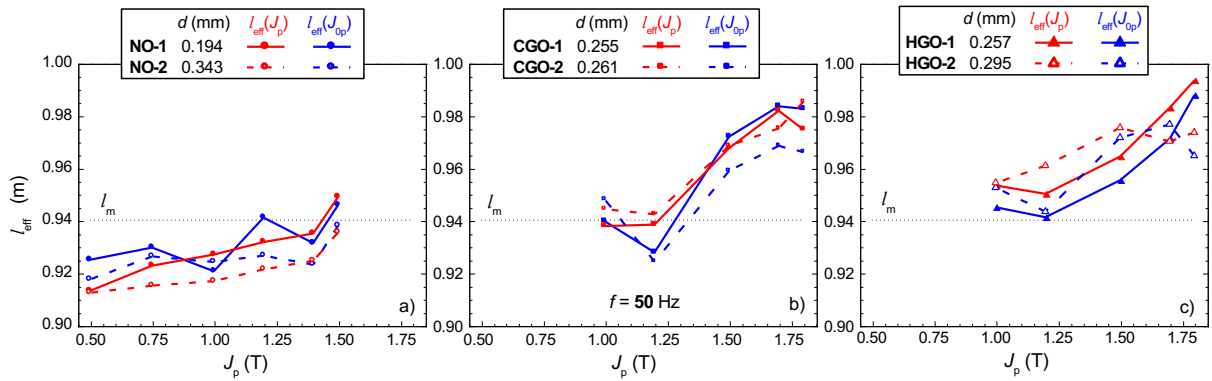


Fig. 5 – The measured effective power loss $P_{\text{eff}}(J_p)$ increases with the peak polarization J_p according to a power law $P_{\text{eff}} \propto J_p^n$, with n an increasing function of J_p .

587
 588
 589
 590
 591
 592
 593
 594
 595
 596



597
 598
 599
 600
 601
 602
 603
 604
 605

Fig. 6 – Effective magnetic path lengths $l_{\text{eff}}(J_{0p})$ and $l_{\text{eff}}(J_p)$ versus peak polarization in the investigated NO and GO steel sheets. $l_{\text{eff}}(J_{0p})$ is calculated through Eqs. (2)–(4). It permits one to retrieve the true power loss value from the standard loss figure for peak polarization J_{0p} measured with the secondary Epstein winding. $l_{\text{eff}}(J_p)$ is the same quantity obtained for $J_p = J_p(0)$, where $J_p(0)$ is the polarization measured at the centre of the Epstein leg.